Songklanakarin J. Sci. Technol.
32 (3), 271-280, May - Jun. 2010

Songklanakarin Journal of Science and Technology
http://www.sjst.psu.ac.th

Original Article

Investigations of spherical grinding parameters on circularity error, finished diameter, and grinding forces for porous polyurethane foam

Isarawit Chaopanich, Somchai Puajindanetr* and Kritdipuk Goyadoolya

Department of Industrial Engineering, Faculty of Engineering,
Chulalongkorn University, Pathum Wan, Bangkok, 10330 Thailand.

Received 24 December 2009; Accepted 29 March 2010

Abstract

The aim of this study was to examine the effect of grinding variables on the circularity error, finished diameter, and grinding forces of porous polyurethane foam (PPUF). A cube of PPUF having the size of 21 mm was transformed into a round shape using a vertical wheel grinding with the circular groove pad developed. The grinding speed (Vs) of the wheel was varied between 1.41 and 5.18 m/s. The cross head speed of the circular groove pad (f) was controlled at 1, 3, 5 mm/min. The abrasive grit size (A) of 20 and 53 μm made of silicon carbide were applied. Two replications of experiment were randomly performed. Diameter and circularity error of the ground specimen were determined by vision measuring machine. The tangential and normal forces of grinding were obtained using a dynamometer. The experimental data were statistically analyzed. The study found that (1) the grinding speed could remarkably affect the circularity error, finished diameter, and grinding forces, (2) the grinding speed ranged between 2.83 and 3.77 m/s could contribute to sphere shape specimens, and (3) the grinding speed of 3.30 m/s, cross head speed of 1 mm/min, and abrasive grit size of 20 μm provided the least circularity error.

Keywords: circularity error, grinding forces, porous polyurethane foam, spherical grinding

1. Introduction

Spherical parts are the most widely used components in many fields of industry, such as silicon nitride ball bearings in automotives and aerospace, porous orbital implants in eyeball surgery, inert ceramic balls used as the covering and supporting materials in reactors in chemical industry, or porous alumina balls in filtration systems. In forming spherical parts, nowadays there have been two main techniques, magnetic fluid grinding and conventional lapping process for high precision ball bearings. Previous research in the field of spherical grinding has mainly focused on the effects of grinding force, rotational speed, and abrasive size on surface damages, surface roughness, sphericity error, and material removal rate of the finished balls for dense materials such as steel and silicon nitride. Stolarski and Tobe (1997) found in the V-groove lapping for silicon nitride balls that a low normal grinding force and a small abrasive particle used contributed to a lower sphericity error with moderate removal rate well agreed with the research of Umehara and Kato (1996) studying magnetic fluid grinding. Kang and Hadfield (2005) showed that increasing some lapping force and speed could give a higher removal rate. However, spherical grinding processes for porous materials have not yet experimentally been revealed. For instance, in spherical orbital implant production, hand grinding by high skilled operators is still needed. Proper grinding conditions suited for the material to be ground have not been set up. As a result, crack damages and a high variation in shape and size occur when uncontrollable directions and high level of grinding forces are applied on the spherical specimen. In the field of porous material machining, there was some recent research that only investigated in orthogonal cutting. Malak and Anderson (2005) showed the effects of cutting tool rake angle, depth of cut,

* Corresponding author.
Email address: fiespj@eng.chula.ac.th

and relative density of polyurethane foam specimen on surface finish, cutting forces, and specific cutting energy. Malak and Anderson (2008) stated that specific cutting energy was reduced by increasing the tool rake angle, cutting speed, and depth of cut for orthogonal cutting of cancellous bone. Chelule *et al.* (2003) studied milling conditions affecting on machined surface of hydroxyapatite ceramic and revealed that the effect of different cutting parameters being cutting speed, feed rate, and depth of cut had insignificant impact on the surface roughness and the sizes of chip fragments removed from the material surface since the microstructure of the material prepared had high porosity and weak grain interfaces.

Therefore, in this study the attempt of finding the influential parameters for spherical grinding via circular groove pad to form spherical shapes in the presence of porous polyurethane foam was firstly presented. Statistical tools including general full factorial design and response surface regression were conducted to examine the significant parameters and to estimate the spherical grinding responses, respectively.

2. Materials and Methods

2.1 Materials

Porous polyurethane foam was introduced as a material in this study, which was characterized for physical and mechanical properties. Pore sizes were estimated via scanning electron microscope (SEM) ranging from 200 to 300 µm. Bulk density was between 0.100 to 0.163 g/cm^3 determined from ASTM D1622-03 Standard Test Method for Apparent Density of Rigid Cellular Plastics. Also, porosity was ranged from 85 to 90%. For mechanical properties, compressive strength, flexural strength and its weibull modulus were 1.05 MPa, 2.14 MPa, and 4.52, which were examined according to ASTM D1621-04a Standard Test Method for Compressive Properties of Rigid Cellular Plastics and ASTM D790-03 Standard Test Methods for Flexural Properties of Unreinforced and Reinforced Plastics and Electrical Insulating Materials, respectively.

2.2 Equipment

Grinding equipment shown in Figure 1 was designed to form a cube specimen to be a spherical finished specimen as expected. Silicon carbide (SiC) sandpaper having grit size of 20 and 53 µm attached to a 125 mm grinding wheel was used as the abrasive tool in the spherical grinding system. The grinding wheel (1) was coupled with the spindle of an AC motor (2) with rated power of 240 Watt and rated speed of 2790 rpm corporate with inverter (3), which was used to adjust grinding speed. A circular groove pad (4) used as a mold to generate spherical finished specimen was attached on a Kistler 9257B dynamometer (5), a 3-component (*Fx, Fy,* and *Fz*) force measurement equipment. The connecting cable of the dynamometer was connected to a charge amplifier (6) to magnify the electrical signal and then sent to a data recorder (7) for data collection and illustration. A universal testing machine was applied to generate elevated cross head speed of the circular groove pad for material removal using a hydraulic power supply system (8) operated by a control unit (9), and the upper frame (10) of the machine was used for the AC motor and grinding wheel installation.

2.3 Experimental methods

2.3.1 Spherical forming

To generate material removal in the spherical grinding system, as-received cube specimen sizing 21 x 21 x 21 mm prepared by saw blade cutting was put into the circular groove pad. It was then elevated by hydraulic power system upward with specified cross head speed to the final head distance of 19.50 mm, which is the distance between the grinding wheel and the bottom of the circular groove. Simultaneously, the silicon carbide grinding wheel with specified speed was operated to grind the specimen. Grinding conditions in terms of grinding speed (Vs, cutting speed), cross head speed (f), and abrasive grit size (A) were set up in Table 1, and two experimental replications were randomly run in fixed effect

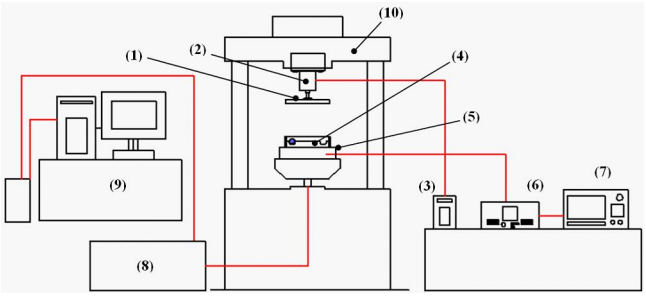

Figure 1. Spherical grinding equipment: (1) grinding wheel, (2) AC motor, (3) inverter, (4) circular groove pad, (5) dynamometer, (6) charge amplifier, (7) data recorder, (8) hydraulic power supply system, (9) control unit, (10) upper frame.

Table 1. Spherical grinding conditions.

Grinding parameters	Range
1. Grinding speed (Vs)	1.41, 2.36, 2.83, 3.30, 3.77, 4.24, 5.18 m/s
2. Cross head speed (f)	1.0, 3.0, 5.0 mm/min
3. Abrasive grit size (A)	20 and 53µm

general full factorial design.

2.3.2 Finished specimen characterizations

After grinding under each condition, finished specimens were visually inspected for their shapes and measured for finished diameter (D) and circularity error (CE) via a vision measuring machine (VMM). Finished diameter (D) of ground specimens referred to the diameter of reference circle in Figure 2 having center point (X_0, Y_0) and radius (r_0) can be examined from all coordinate points of circular feature. Four main techniques such as minimum circumscribed circle (MCC), maximum inscribed circle (MIC), minimum zone solution (MZS), and least square circle (LSC) can be applied to determine reference circle. The error of the reference circle with respect to the *i*th point (X_i, Y_i) is given by Equation 1.

$$e_i = \sqrt{(X_i - X_0)^2 + (Y_i - Y_0)^2} - r_0 \quad (1)$$

The difference between the maximum value (e_{max}) and minimum value (e_{min}) among these errors is defined as the circularity error (*CE*) expressed in Equation 2 (Dhanish and Mathew, 2006).

$$CE = e_{max} - e_{min} \quad (2)$$

In the ISO 3290, circularity error is measured in two or three equatorial planes at 90° to each other (Wen and Song, 2004). In this work, four measurements for each finished specimen were taken and the average values were used in the analysis.

2.3.3 Grinding force measurement

Grinding force components (*Fx, Fy,* and *Fz*) exerted to the dynamometer from the beginning to the end of the grinding run were sent to data recorder. The tangential force (*Ft*) acting in the direction of cutting is the resultant of the *Fx* and *Fy* force component as expressed in Equation 3, and the normal force (*Fn*) vertically normal to cutting direction is presented as Fz force component in Equation 4. All tangential forces (Ft_1, Ft_2, ..., Ft_n) and normal forces (Fn_1, Fn_2, ..., Fn_n) for each grinding condition were calculated in terms of root mean square (RMS) in Equation 5, which was used in the analysis.

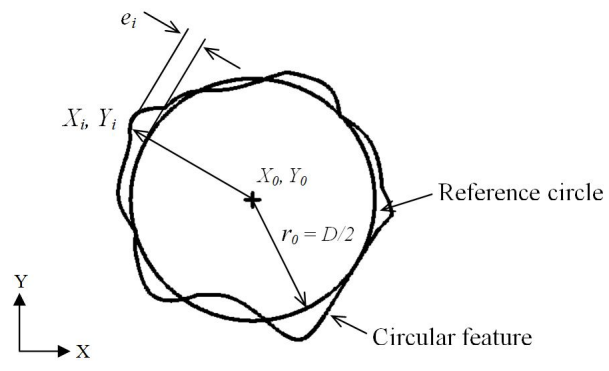

Figure 2. Reference circle.

$$Ft = \sqrt{Fx^2 + Fy^2} \quad (3)$$

$$Fn = Fz \quad (4)$$

$$Ft,n_{RMS} = \sqrt{\frac{1}{n}\sum_{i}^{n}(Ft,n)_i^2} \quad (5)$$

2.3.4 Statistical analysis

Analysis of variance (ANOVA) was used to examine the effects of grinding parameters including grinding speed, cross head speed, and abrasive grit size as well as their interactions on grinding responses; circularity error, finished diameter, tangential force, and normal force via Minitab statistical software. Main effects and interactions were graphically demonstrated. P-value and percent contribution of mean square were also summarized to indicate the significant grinding parameters. Significance level (α) was set to be 0.05. In addition, the experimental results were used to develop second order response surface regression models expressed as Equation 6 to estimate grinding responses (y) through the set of variables ($x_1, x_2, ..., x_n$).

$$y = b_0 + \sum_{i=1}^{n} b_i x_i + \sum_{i=1}^{n} b_{ii} x_i^2 + \sum\sum_{i<j} b_{ij} x_i x_j + \varepsilon \quad (6)$$

where ε represents the error observed in the response y and *b's* are the regression coefficients (Montgomery, 2001).

3. Results and Discussion

3.1 Finished shape and circularity error

Table 2 summarizes finished shapes of the ground specimen from all grinding conditions. It was found that egg shapes in Figure 3 (a) were formed at the lowest grinding speed of 1.41 m/s. Meanwhile, grinding speeds from 2.83 to 3.77 m/s contributed to sphere shapes in Figure 3 (b) for all cross head speeds and abrasive grit sizes. At the highest level grinding speed of 5.18 m/s, partial sphere and squircle shapes in Figure 3 (c) and (d) were formed. Moreover, for grinding speeds of 2.36 and 4.24 m/s, egg, sphere, and partial sphere shapes emerged at some levels of cross head speeds and abrasive grit sizes.

Along with shape consideration, circularity errors examined from VMM were graphically depicted by means of a dot plot in Figure 4. From the plot, circularity errors below 0.625 mm contributed to all sphere shapes formed, discriminating sphere shape from the others. Furthermore, sphere, partial sphere, and squircle shapes could be formed for circularity errors approximately above 0.625 to 0.75 mm because of visual determination for finished shapes. However, descrip-

Table 2. Results of finished shapes after grinding.

Cross head speed; f		Abrasive grit size; A											
		20 µm						53 µm					
		1.0 mm/min		3.0 mm/min		5.0 mm/min		1.0 mm/min		3.0 mm/min		5.0 mm/min	
		R1	R2	R1	R2	R1	R2	R1	R2	R1	R2	R1	R2
Grinding speed; Vs	1.41 m/s	E	E	E	E	E	E	E	E	E	E	E	E
	2.36 m/s	S	S	S	S	E	E	S	S	S	S	E	E
	2.83 m/s	S	S	S	S	S	S	S	S	S	S	S	S
	3.30 m/s	S	S	S	S	S	S	S	S	S	S	S	S
	3.77 m/s	S	S	S	S	S	S	S	S	S	S	S	S
	4.24 m/s	S	S	S	S	S	S	P	P	S	S	S	S
	5.18 m/s	P	P	SQ	P	P	P	SQ	SQ	P	P	P	P

Remarks: R1, R2 = Experimental replication 1, 2; E = Egg; S = Sphere; P = Partial sphere; SQ = Squircle.

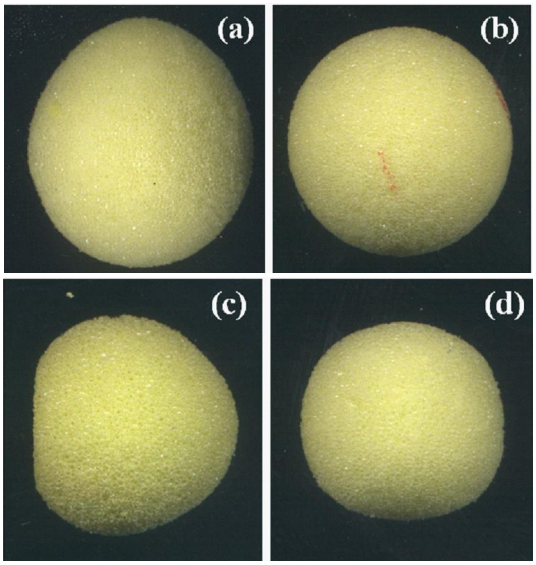

Figure 3. Various finished shapes: (a) egg, (b) sphere, (c) partial sphere, and (d) squircle.

tive statistics in terms of minimum, mean, maximum, standard deviation, coefficient of variation, and confidence interval of circularity error for various shapes are demonstrated in Table 3. The sphere shape of the specimens provided the lowest circularity error in average of 0.59±0.07 mm, and also the 95% confidence interval with the range of 0.57 and 0.61 mm.

In addition, main effect and interaction plots are illustrated in Figure 5 (a) and (b). In the main effect plots, circularity error rapidly dropped from 1.57 mm to the lowest point of 0.56 mm when increasing grinding speed from 1.41 to 3.30 m/s, then rising again to reach 1.05 mm for grinding speed of 5.18 m/s. Increasing cross head speed from 1.0 to 5.0 mm/min increased circularity error while increasing abrasive grit size had no remarkable effect. Grinding speed of 3.30 m/s, cross head speed of 1.0 mm/min, and abrasive grit size of 20 µm seemed to be the optimal condition, providing minimum circularity error.

Results from analysis of variance in Table 4 illustrate that grinding speed (Vs) was the most influential parameter with 76% contribution. However, cross head speed (f), interaction between grinding speed and cross head speed (Vs*f),

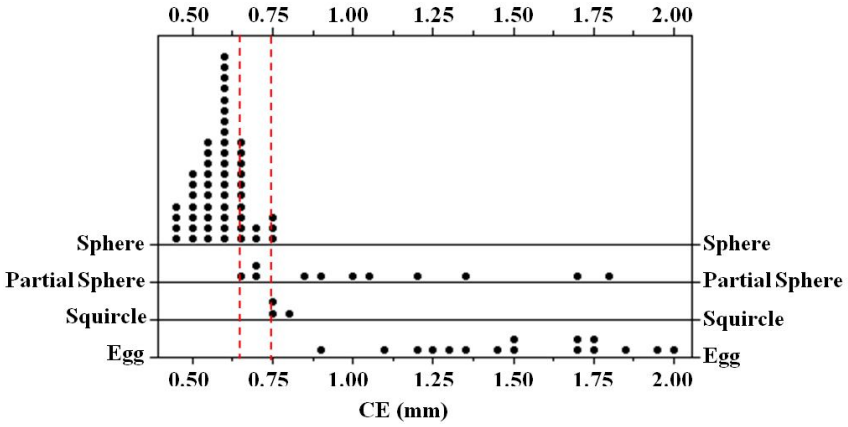

Figure 4. Dot plot of circularity error for various shapes.

Table 3. Descriptive statistics summary of circularity error (mm) for various shapes.

Shape	Min.	Mean	Max.	SD	CV	95% C.I.	N
Egg	0.89	1.51	1.98	0.32	20.8%	[1.35, 1.68]	16
Sphere	0.46	0.59	0.76	0.07	12.0%	[0.57, 0.61]	54
Partial Sphere	0.64	1.08	1.81	0.40	37.2%	[0.81, 1.35]	11
Squircle	0.77	0.78	0.78	0.01	0.9%	[0.76, 0.79]	3
ALL							84

Remarks: Min. and Max. = Minimum and maximum value; SD = Standard deviation; CV = Coefficient of variation; C.I. = Confidence interval; N = Number of specimen.

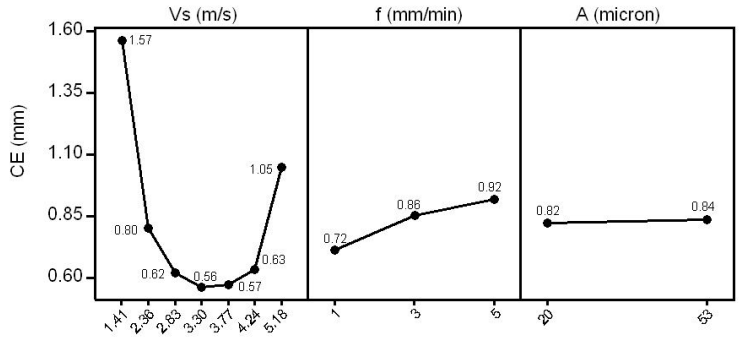

(a) Main effect plots for circularity error (CE).

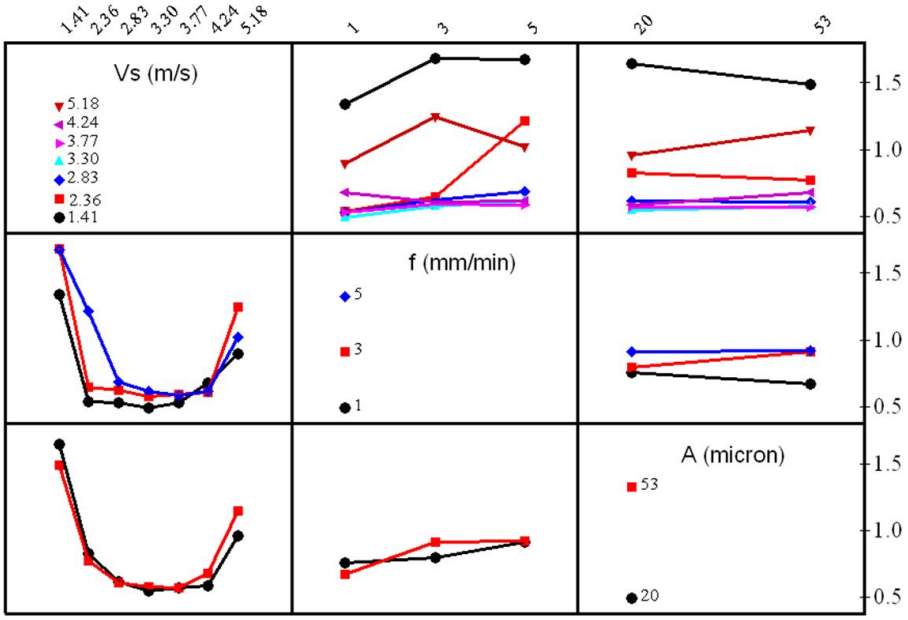

(b) Interaction plots for circularity error (CE).

Figure 5. Main effect plots (a) and interaction plots (b) for circularity error.

interaction between grinding speed and abrasive grit size (Vs*A), interaction between cross head speed and abrasive grit size (f*A), and interaction of the three parameters (Vs*f *A) were also significant regarding P-value less than 0.05. Moreover, the experimental results were used to develop the mathematical model to estimate circularity error via second order response surface regression as shown in Equation 7. This model was found to be significant with P-value less than 0.05 and R-square of 81.6%.

For spherical surface generation mechanism, it was

Table 4. Results of P-value and percent contribution from analysis of variance for CE, D, Ft, and Fn.

Source	CE		D		Ft		Fn	
	P-value	%Contr.	P-value	%Contr.	P-value	%Contr.	P-value	%Contr.
Vs	<0.0001*	76%	<0.0001*	40%	<0.0001*	55%	<.0001*	63%
f	<0.0001*	5%	0.0022*	5%	0.0013*	17%	0.0011*	12%
A	1.0000	0%	<0.0001*	23%	0.0075*	17%	0.0012*	18%
Vs*f	<0.0001*	8%	<0.0001*	10%	0.6687	2%	0.8324	1%
Vs*A	0.0051*	2%	<0.0001*	9%	0.7379	1%	0.6252	1%
f*A	0.0172*	1%	0.0004*	7%	0.1283	5%	0.3008	2%
Vs*f*A	<0.0001*	7%	<0.0001*	5%	0.623	2%	0.3285	2%
Error		0%		1%		2%		2%

Remarks: * = Significant; %Contr. = Percent contribution.

observed from the experiment that the specimens ground with low grinding speed (1.41 to 2.36 m/s) did not rotate across their own axes, but just orbited and plowed around the groove with low speeds. As a result, large finished size and high circularity error of the ground specimen occurred after grinding. The specimens ground with grinding speed between 2.83 and 3.77 m/s were induced to skid across their axes and to change their positions while rotating around the groove, promoting more ground surface area with random positions and consecutively resulting in the ground specimen with minimal circularity error. At high grinding speed above 4.24 m/s, the ground specimens were induced to rotate around the groove too fast to change their positions randomly in the contact between the specimen, circular groove, and grinding wheel. This resulted in small finished sizes and high circularity errors. The greater the grinding area, the higher possibility of forming sphere shape corresponded to the previous work of Lee *et al.* (2006) and Stolarski (1999) who stated that to receive the roundness ball, the motion of a ball should be random, and the orientation of the ball being ground should be different to its previous orientation.

$$CE = 3.23 - 1.60Vs + 0.21f - 0.012A + 0.22Vs^2 - 0.007f^2 - 0.038Vs*f + 0.003Vs*A + 0.0004f*A \quad (7)$$

3.2 Finished diameter

To investigate the effects of grinding parameters on finished diameter, the main effect and interaction of data mean are plotted in Figure 6 (a) and (b). It was shown in the main effect plots that finished diameters dramatically decreased as increasing grinding speed from 1.41 to 2.83 m/s and 4.24 to 5.18 m/s. A gradual decrease in finished diameter from 19.31 to 19.20 mm was performed for a grinding speed between 2.83 and 4.24 m/s. Reduction in finished diameter when increasing the grinding speed can be explained by Archard's wear equation that material removal rate is directly proportional to sliding speed of an abrasive process (Liu and Li, 2001).

In addition, grinding with larger abrasive grit size contributed to more penetrate depth of cut resulting in higher material removal rate and consequently smaller finished diameter. Statistical results in Table 4 indicate that all grinding parameters and their interactions were significant with P-value less than 0.05. Grinding speed was the most influential parameter with 40% contribution, followed by abrasive grit size with 23% contribution.

Regarding all finished sphere shapes formed with grinding speed between 2.83 to 3.77 m/s for all cross head speeds and abrasive grit sizes, experimental results in this range were used to construct a response surface regression model as shown in Equation 8. The model was reported to be significant with P-value less than 0.05 and R-square of 72.8%.

$$D = 19.21 + 0.27 \cdot Vs - 0.115 \cdot f - 0.003 \cdot A - 0.053 \cdot Vs^2 - 0.012 \cdot f^2 + 0.005 \cdot Vs \cdot f + 0.0005 \cdot Vs \cdot A - 0.0001 \cdot f \cdot A \quad (8)$$

3.3 Tangential force

The main effect and interaction of data means of tangential force for all grinding conditions are shown in Figure 7 (a) and (b). It was found that tangential force substantially decreased as grinding speed increased from 1.41 to 5.18 m/s, but had a slightly upward trend when increasing cross head speed from 1.0 to 5.0 mm/min. This is well agreed with much previous work of Malkin and Hwang (1996), Yui and Lee (1996), Ramesh *et al.* (2001), Shen *et al.* (2002), Tang *et al*. (2009), and Yallese *et al.* (2009) in conventional surface grinding. In addition, grinding with smaller abrasive grit size contributed to greater tangential force, different from much research presented by Liu *et al.* (2001) and Qi *et al.* (1997) for dense materials. In general, a larger abrasive grit size in grinding leads to a greater depth of cut and results in greater grinding forces. But when considering in depth, microstructure and mechanical properties of dense materials are very homogeneous and higher than those of porous materials.

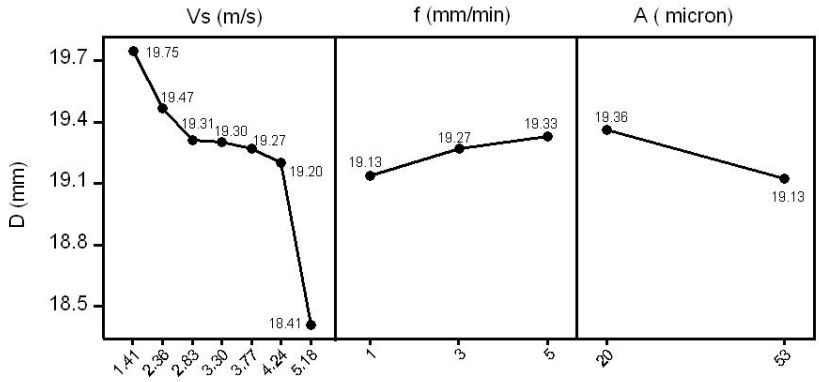

(a) Main effect plots for finished diameter (D).

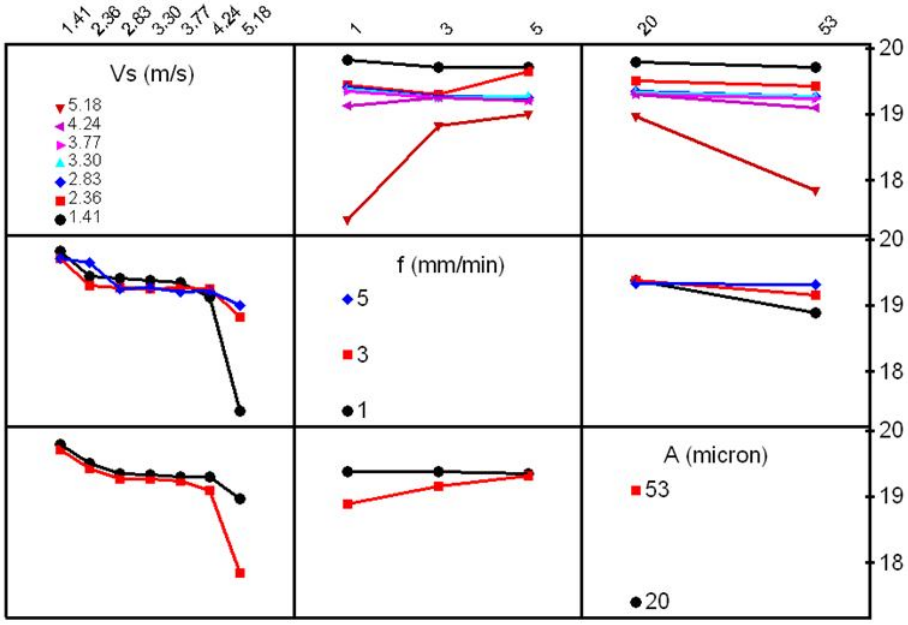

(b) Interaction plots for finished diameter (D).

Figure 6. Main effect plots (a) and interaction plots (b) for finished diameter.

Consequently, insignificant variation in grinding force can be received for grinding dense materials. Moreover, Kalpakjian and Schmid (2001) stated that not only grinding conditions such as cutting speed, feed rate, and depth of cut, but also the strength of materials being ground can affect grinding force for material removal processes.

From the results in Table 4, the three grinding parameters including grinding speed (Vs), cross head speed (f), and abrasive grit size (A) were statistically significant with P-value less than 0.05, while their interactions were found to be not significant. Grinding speed was the most influential parameter with 55% contribution, followed by cross head speed and abrasive grit size with 17% contribution.

To estimate the tangential force in the spherical grinding system, a second order response surface regression model was developed from experimental results and presented in Equation 9. Analysis of variance indicated that the model was significant with P-value less than 0.05 and R-square of 74.8%.

$$Ft = 0.48 - 0.14 \cdot Vs + 0.03 \cdot f - 0.003 \cdot A + 0.015 \cdot Vs^2 - 0.002 \cdot f^2 - 0.006 \cdot Vs \cdot f + 0.0002 \cdot Vs \cdot A + 0.0004 \cdot f \cdot A \quad (9)$$

3.4 Normal force

The main effect and interaction plots of data means in Figure 8 (a) and (b) show that the normal force declined as the grinding speed increased from 1.41 to 5.18 m/s, but inversely increased when increasing the cross head speed from 1.0 to 5.0 mm/min. Grinding with smaller abrasive grit size gave higher normal force. Normal force in the spherical grinding system performed as the same pattern as tangential force. As can be seen in Table 4, results from ANOVA show

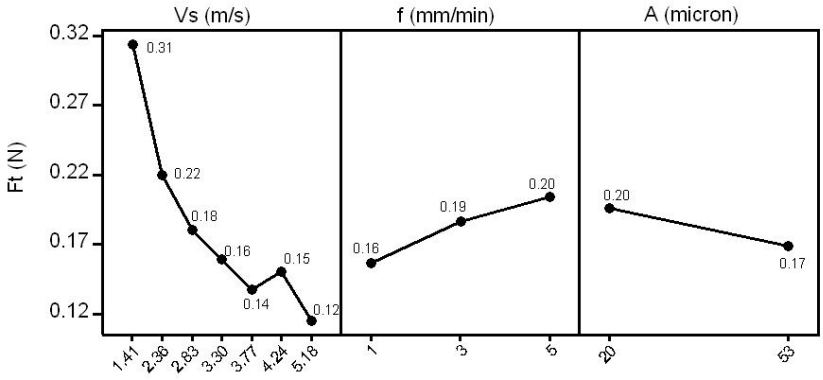

(a) Main effect plots for tangential force (Ft).

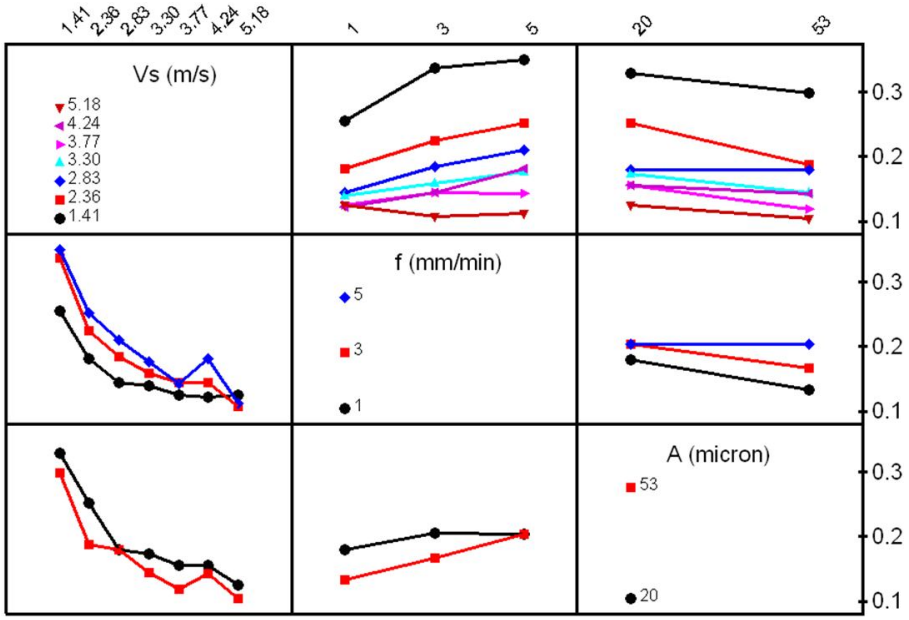

(b) Interaction plots for tangential force (Ft).

Figure 7. Main effect plots (a) and interaction plots (b) for tangential force.

that grinding speed, cross head speed, and abrasive grit size significantly influenced normal force with a P-value less than 0.05. Grinding speed was the most significant parameter with 63% contribution, followed by the abrasive grit size and cross head speed with 18% and 12% contribution, respectively.

Moreover, to estimate the normal force in terms of grinding parameters for the spherical grinding system, a second order response surface regression model is expressed in Equation 10 and found to be significant with P-value less than 0.05 and R-square of 81.2%.

$$Fn = 0.50 - 0.14 \bullet Vs + 0.03 \bullet f - 0.002 \bullet A + 0.013 \bullet Vs^2 - 0.001 \bullet f^2 - 0.005 \bullet Vs \bullet f + 0.0001 \bullet Vs \bullet A + 0.0003 \bullet f \bullet A \quad (10)$$

4. Conclusions

In this study, finished shape, circularity error, finished diameter of the ground specimen, and grinding forces in spherical grinding porous polyurethane foam using circular groove pad were investigated. Conclusions of the results are drawn as following:

1. Sphere shapes of finished specimen could be formed with the range of the circularity error between 0.57 and 0.61 mm and 95% confidence interval.

2. Grinding speed, cross head speed, interaction between grinding speed and cross head speed, interaction between grinding speed and abrasive grit size, interaction between cross head speed and abrasive grit size, and interaction of the three parameters significantly affected circularity error of the ground specimen.

3. All grinding parameters, including grinding speed, cross head speed, abrasive grit size, and their interactions significantly influenced the finished diameter. In addition, gradual decrease in finished diameter occurred for grinding speed between 2.83 to 4.24 m/s.

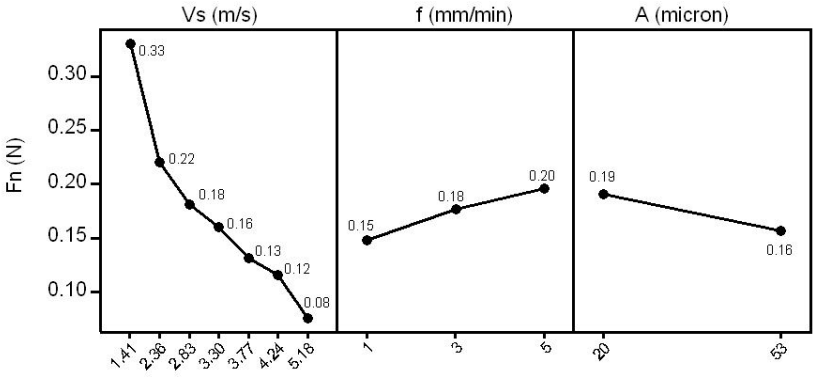

(a) Main effect plots for normal force (Fn).

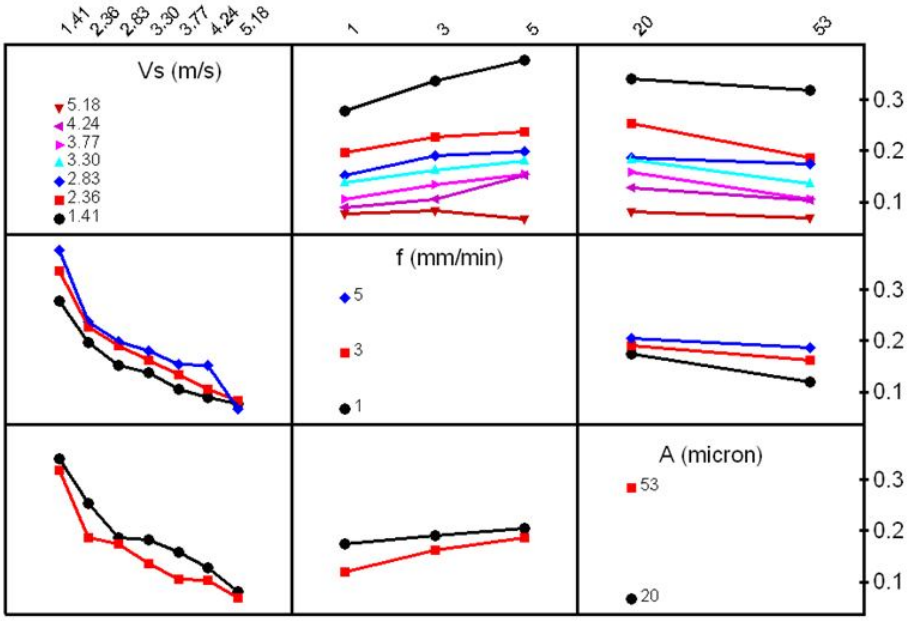

(b) Interaction plots for normal force (Fn).

Figure 8. Main effect plots (a) and interaction plots (b) for normal force.

4. Tangential force and normal force were influenced by grinding speed, cross head speed, and abrasive grit size.

5. Grinding speed was the most significant parameter, influencing circularity error, finished diameter, tangential force, and normal force with percent contributions of 76%, 40%, 55%, and 63%, respectively.

6. The grinding speed between 2.83 and 3.77 m/s could form the spherical work pieces whereas the grinding speed of 3.30 m/s, cross head speed of 1.0 mm/min, and abrasive grit size of 20 μm provided the minimum circularity error.

Acknowledgements

The work described in this paper was fully supported by the Department of Industrial Engineering, Faculty of Engineering and the Graduate School, Chulalongkorn University, Thailand. The authors also thank C. Dumkum from the Department of Industrial Engineering, Faculty of Engineering, King Mongkut's University of Technology Thonburi, Thailand, for the use of the vision measuring machine.

References

ASTM D790-03. 2003. Standard Test Methods for Flexural Properties of Unreinforced and Reinforced Plastics and Electrical Insulating Materials, American Society for Testing and Materials, West Conshohocken, Pennsylvania, U.S.A.

ASTM D1621-04a. 2004. Standard Test Method for Compressive Properties of Rigid Cellular Plastics, American Society for Testing and Materials, West Conshohocken, Pennsylvania, U.S.A.

ASTM D1622-03. 2003. Standard Test Method for Apparent Density of Rigid Cellular Plastics, American Society for Testing and Materials, West Conshohocken, Pennsylvania, U.S.A.

Chelule, K.L., Coole, T.J. and Cheshire, D.G. 2003. An investigation into the machinability of hydroxyapatite for bone restoration implants. Journal of Materials Processing Technology. 135, 242-246.

Dhanish, P.B. and Mathew, J. 2006. Effect of CMM point coordinate uncertainty on uncertainties in determination of circular features. Measurement. 39, 522-531.

ISO 3290. 1975. Rolling bearings-bearing parts-ball for rolling bearings, International Organization for Standardization, Geneva, Switzerland.

Kalpakjian, S. and Schmid, S.R. 2001. Manufacturing Engineering and Technology, 4th Edition, Prentice Hall Inc, New Jersey, U.S.A.

Kang, J. and Hadfield, M. 2005. Examination of the material removal mechanisms during the lapping process of advanced ceramic rolling elements. Wear. 258, 2-12.

Lee, R.T., Hwang, Y.C. and Chiou, Y.C. 2006. Lapping of ultra-precision ball surfaces part I: Concentric V-groove lapping system. International Journal of Machine Tools and Manufacture. 46, 1146-1156.

Liu, R. and Li, D.Y. 2001. Modification of Archard's equation by taking account of elastic/pseudoelastic properties of materials. Wear. 251, 956-964.

Liu, T., Latella, B.A. and Zhang, L. 2001. Grinding of Ceramics: Strength, Surface Features and Grinding Conditions. Key Engineering Materials. 196, 53-60.

Malak, S.F.F. and Anderson, I.A. 2005. Orthogonal cutting of polyurethane foam. International Journal of Mechanical Sciences. 47, 867-883.

Malak, S.F.F. and Anderson, I.A. 2008. Orthogonal cutting of cancellous bone with application to the harvesting of bone autograft. Medical Engineering & Physics. 30, 717-724.

Malkin, S. and Hwang, T.W. 1996. Grinding Mechanisms for Ceramics, Annals of the ClRP, Vol. 45/2.

Montgomery, D.C. 2001. Design and Analysis of Experiments, John Wiley & Sons, New York, U.S.A., pp. 427.

Qi, H.S., Rowe, W.B. and Mills, B. 1997. Experimental investigation of contact behavior in grinding. Tribology Intemational. 30, 283-294.

Ramesh, K., Yeo, S.H., Gowri, S. and Zhou, L. 2001. Experimental Evaluation of Super High-Speed Grinding of Advanced Ceramics. International Journal of Advanced Manufacturing Technology. 17, 87-92.

Shen, J., Luo, C., Zeng, W., Xu, X. and Gao, Y. 2002. Ceramic grinding under constant pressure. Journal of Materials Processing Technology. 129, 176-181.

Stolarski, T.A. and Tobe, S. 1997. The effect of accelerated material removal on roundness and residual stresses in ceramic balls. Wear. 205, 206-213.

Stolarski, T.A. 1999. Mechano-chemical wear of ceramics. Journal of Materials Science. 34, 3609-3622.

Tang, J., Du, J. and Chen, Y. 2009. Modeling and experimental study of grinding forces in surface grinding. Journal of Materials Processing Technology. 209, 2847-2854.

Umehara, N. and Kato, K.1996. Magnetic fluid grinding of advanced ceramic balls. Wear. 200, 148-153.

Wen, X. and Song, A. 2004. An immune evolutionary algorithm for sphericity error evaluation. International Journal of Machine Tools and Manufacture. 44, 1077-1084.

Yallese, M.A., Chaoui, K., Zeghib, N., Boulanouar, L. and Rigal, J.F. 2009. Hard machining of hardened bearing steel using cubic boron nitride tool. Journal of Materials Processing Technology. 209, 1092-1104.

Yui, A. and Lee, H. 1996. Surface grinding with ultra high speed CBN wheel. Journal of Materials Processing Technology. 62, 393-396.